

Coverage dependence of Sb/Si(111) adsorption and desorption modes: Interplay between chemical interactions and site transitions

H. Guesmi,^{1,*} L. Lapena,^{1,2} G. Tréglia,¹ and P. Müller^{1,2}

¹Aix Marseille Université, Centre de Recherche sur la Matière Condensée et les Nanosciences, UPR CNRS Associé aux Universités Aix Marseille II et III, Campus de Luminy, case 913, F-13288 Marseille Cedex 9, France

²Université Paul Cézanne-Aix Marseille III, 3 Av. R. Schuman, 13628 Aix en Provence, France

(Received 29 August 2007; revised manuscript received 31 October 2007; published 1 February 2008)

The kinetic and thermodynamic properties of adsorption and desorption of Sb onto a Si(111) surface are analyzed by mass spectrometry and *ab initio* calculations. Two domains of temperature are evidenced. At $T < 600$ °C there is an irreversible adsorption involving a subtle competition between sticking, adsorption, then dissociation of Sb_4 tetramers associated to a partial reflection of Sb_4 molecules on the Sb-covered surface. At $T > 800$ °C, Sb_4 molecules are dissociated close to the surface leading to a simple reversible adsorption/desorption of Sb monomers. In this temperature range, adsorption/desorption isotherms can be recorded for various temperatures, which reveal a surprising behavior since quasi-Langmuir isotherms appear to be the consequence of a two-dimensional (2D) phase transition. More precisely, as shown by *ab initio* calculations, during the submonolayer adsorption process, the adsorption site evolves (as a function of coverage) from ternary towards on-top position and the character of the Sb-Sb effective interactions changes from repulsive towards attractive. The 2D phase transition close to $\theta \approx 0.7$ ML seems to be associated to characteristic signatures in many other experiments. Then for high enough supersaturations, it is possible to overpass $\theta = 1$ ML by the formation of dimers, first partially located on top sites which repel one another, up to a second phase transition around $\theta = 1.3$ ML in which dimers leave the on top sites and stand up to occupy almost vertically the hollow ones for building the second Sb layer. Lastly surfactant effect is quantified.

DOI: [10.1103/PhysRevB.77.085402](https://doi.org/10.1103/PhysRevB.77.085402)

PACS number(s): 68.35.Rh, 68.35.Md, 68.43.Bc, 47.55.dk

I. INTRODUCTION

Due to the role played by antimony both as a doping of silicon¹ and a surfactant in molecular beam epitaxy,² there has been a wide interest in the study of the Sb-Si interaction. Most of the older experimental results concern the kinetics of the adsorption on Si(001) surfaces.^{3–5} However, some experiments concerning Si(111) surfaces have been reported. More precisely Metzger *et al.*⁶ evidenced two adsorption modes: a two-dimensional (2D) one at $T > 600$ °C and a 3D one at $T < 500$ °C, respectively, characterized by a first order and a zero order desorption. Later, Andrieu *et al.*⁷ focused on the study of the 2D adsorption mode, which appears to be typical of a monomer Sb adsorption at temperatures higher than 725 °C but proceeds by Sb_4 physisorption followed by dissociation on the surface at lower temperature. More recent studies are focused on scanning tunneling microscopy (STM) studies of the various 2D phases that may appear according to the experimental conditions of temperature and surface coverage.^{6–12}

All these studies open new questions. It is in particular the case of the nature of the relevant entities (monomers, dimers, trimers, or tetramers) which, according to the temperature, can play different roles on the sticking coefficient and on the adsorption and desorption mechanisms (from both kinetics and thermodynamic points of view). It is also the case of the link between the various superstructures described in the literature and the true equilibrium phase diagram. Last but not least, the nature of the antimony adsorption (molecular or dissociative adsorption) as well as the nature of the adsorbed Sb particle interactions has still to be understood. The better way to explore the diversity of the mechanisms and to estab-

lish a link between kinetics, thermodynamics, and the various superstructures described in the literature was to perform a systematic study of the adsorption and desorption properties in a large domain of temperature and in- and out-of-equilibrium conditions.

Our first steps in the study of this system concerned the incorporation properties of Sb in bulk silicon with the simple idea to use vicinal Si surfaces to facilitate the Sb incorporation at the step edges. Surprisingly, we found just the reverse, the antimony incorporation being more difficult at the step edges than on the terraces.¹³ The interpretation was found by a first thermodesorption approach coupled to quenched molecular-dynamics calculations: there was a molecular (dimers) adsorption at the steps instead of a dissociative (monomers) one on the terraces.¹⁴ We thus decided to go beyond these preliminary results (obtained with partially inadequate description of the Sb-Si potential) that means: (i) revisit the adsorption and desorption kinetics in a large temperature range,¹⁵ (ii) measure the Sb/Si(111) isotherms for having access to all the thermodynamic properties of this system,¹⁶ (iii) use *ab initio* calculations to obtain more accurate atomic potentials and thus a more accurate description of the atomistic mechanisms that occur at the Si surface, and (iv) use the so-obtained potential and Monte Carlo simulations to analyze the whole behavior in the presence of a Sb vapor.

In this paper are summarized the results corresponding to the points (i)–(iii) (the results corresponding to the last point (iv) will be published elsewhere¹⁷). Our results evidence that the physics of the adsorption and desorption mechanisms of Sb/Si(111) is much more rich than expected. In particular, it is found that the nature of the atomic interactions change

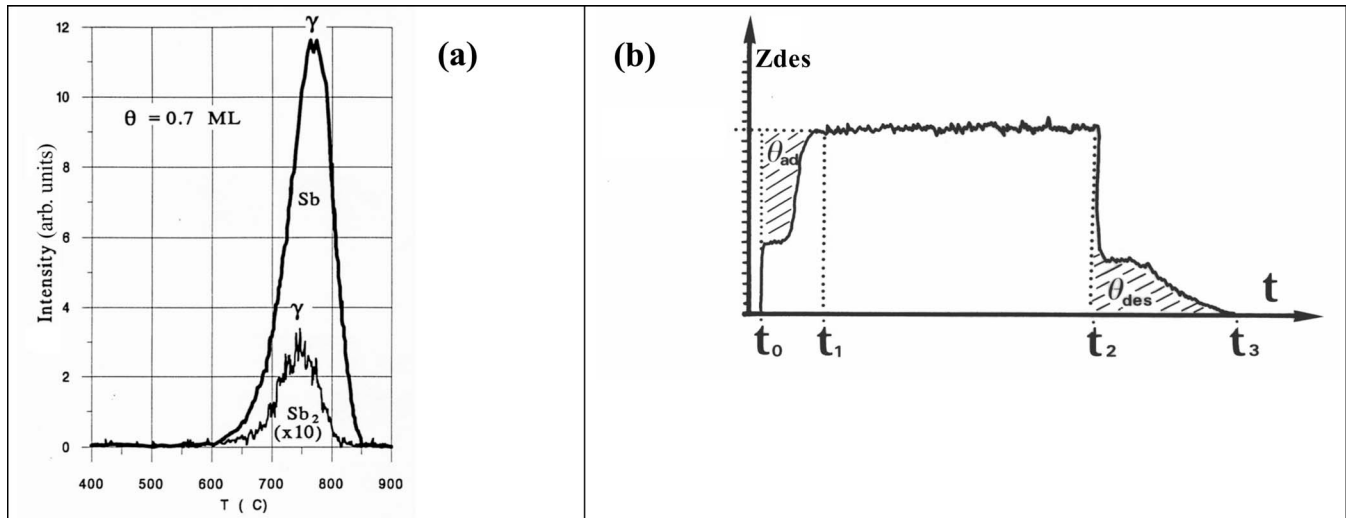


FIG. 1. (a) Thermodesorption spectrum recorded for the $\theta \approx 0.7$ ML antimony monolayer deposited at 400°C on the Si(111) surface and (b) typical mass spectrometry experiment.

with the surface coverage (from vanishing toward attractive interactions in experiments, from repulsive toward attractive interactions in calculations).

The paper is divided into five sections: Section II is devoted to the description of the specific experiments, Sec. III deals with the description of the adsorption and desorption mechanism (with a particular emphasis for the kinetics), in Sec. IV the equilibrium properties are studied *via* adsorption and desorption isotherms, Sec. V concerns the structural study of the 2D equilibrium phases, and lastly, Sec. VI is devoted to *ab initio* calculations. Lastly, a short conclusion gives some perspectives.

II. DESCRIPTION OF THE EXPERIMENTS

A. Experimental description

Adsorption and desorption properties of antimony on a Si(111) surface can be obtained by mass spectrometry measurements completed by reflection high energy electron diffraction (RHEED) studies giving access to the crystallographic structures of the structural phases existing in and out of equilibrium conditions. For this purpose we use an experimental setup described elsewhere.¹⁸

The mass spectrometer (MS) we use is a quadrupolar Balzers QMG 420 spectrometer which, because of the excitation energy, partially dissociates the Sb_4 molecules in Sb_2 dimers and Sb monomers. The MS calibration of the dissociation coefficient is measured by directly sending Sb_4 molecules from the Knudsen cell in the MS chamber, then measuring the so-induced Sb_n flux. It is found that a pure Sb_4 flux is characterized by a ratio $Z_{\text{Sb}}/Z_{\text{Sb}_2} \approx 1.5 \pm 0.1$ where Z_{Sb} and Z_{Sb_2} , respectively, are Sb and Sb_2 recorded flux. In our experimental conditions (and after correction of a calibration factor), it means that, when a Sb_4 molecule is collected by the MS, it is dissociated in 3.44 monomers and 0.56 dimer atoms.

The silicon wafer we use is of p type (boron doped) with a resistivity $\rho \approx 1 \Omega \text{cm}^{-1}$. The samples are introduced in the

experiment chamber after standard cleaning procedure (alcohol then acetone and ultrasonic bath) then cleaned in the ultrahigh vacuum chamber by a thermal flash (1250°C during a few seconds) then annealed (1000°C during half an hour) in order to favor the appearance of large terraces between step bunches. Antimony is a commercial one (purity 99.9999%). It is evaporated from a Knudsen cell situated at 2 cm from the silicon surface. In the so-used conditions, the impinging flux essentially contains Sb_4 tetramers.

B. Experimental procedure

Two kinds of mass spectrometry experiments can be performed: thermodesorption or steady state measurements. Two typical spectra are reported in Fig. 1.

(1) For thermodesorption spectrometry (TDS) measurements, antimony is deposited at $T=T_0$ (in fact at low temperature), then the substrate is heated using a linear temperature ramp (heating rate: 4 K/s). In Fig. 1(a) is reported the TDS spectrum recorded for 0.7 ML of Sb deposited at RT. There is no desorption before $T=600^\circ\text{C}$, then the desorbed signal reaches its maximum for roughly $T=775^\circ\text{C}$. More precisely, the desorption peak (labeled γ) that exists for $\theta < 0.7$ ML splits into two components at $\theta \approx 0.7$ ML. The relative intensities of both components then vary *versus* the excess coverage from 1 (at $\theta \approx 0.7$ ML as seen in Fig. 1(a) where the splitting is just beginning) to 1/2 at $\theta \approx 1$ ML (not shown). Furthermore, notice that even if most of the desorbed signal consists of Sb species, a very weak amount of Sb_2 species also contributes to the desorption. In this peculiar case, we have shown that these additional Sb_2 species originate from step edges.¹⁴

(2) Steady-state experiments consist of measuring the molecular flux leaving the surface at a fixed temperature T_s in the presence then in the absence of an impinging antimony flux. In Fig. 1(b) is sketched a typical curve furthermore obtained in reversible adsorption/desorption conditions. More precisely, we report the flux $Z \uparrow$ leaving the surface

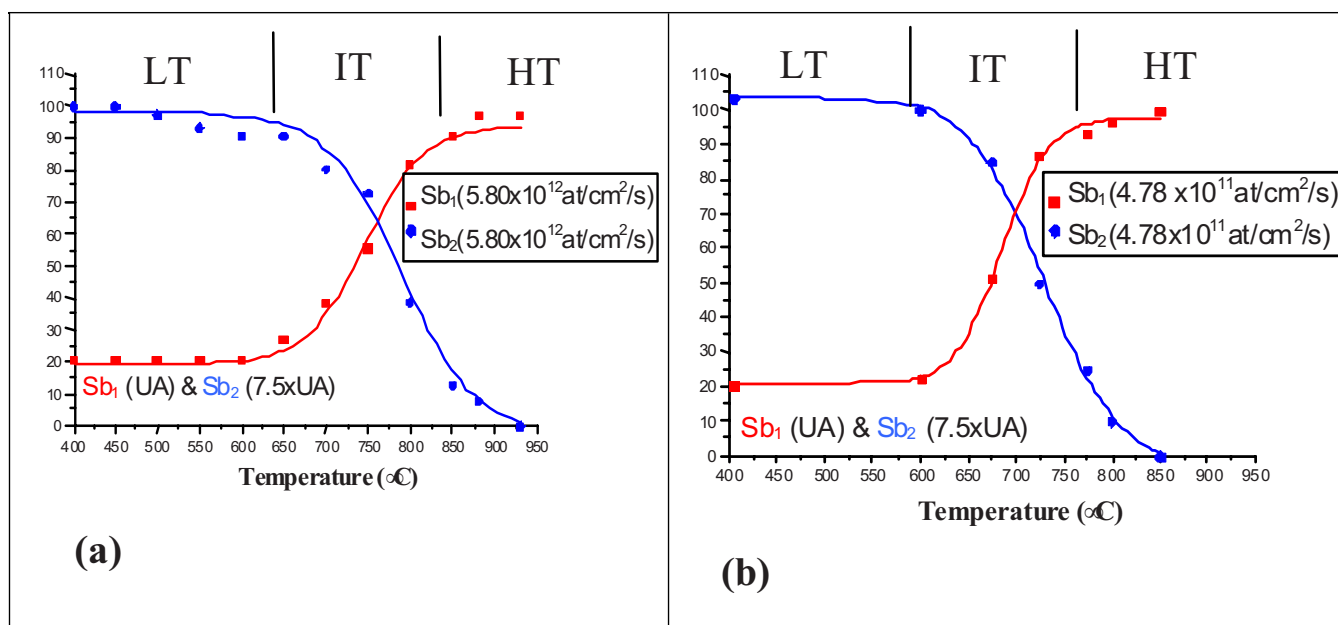


FIG. 2. (Color online) Intensities Z_{Sb} and Z_{Sb_2} of Sb and Sb_2 species leaving the crystal versus the substrate temperature. The impinging flux is $Z_{\downarrow} = 5.80 \times 10^{12}$ at $s^{-1} cm^{-2}$ in Fig. 2(a) but $Z_{\downarrow} = 4.78 \times 10^{11}$ at $s^{-1} cm^{-2}$ in (b). Notice that the position of the crossing point slightly varies with the impinging flux.

versus the deposit time t . Let us describe the general form of this curve. At $t=t_0$ the shutter in front of the Knudsen cell is opened so that the leaving flux abruptly increases to $(1-\alpha_0)Z_{\downarrow}$ which corresponds to the fraction of the incident flux Z_{\downarrow} reflected on the surface (α_0 thus is the sticking coefficient at zero coverage). After a transitory period ($t=t_1$), the leaving flux reaches a steady state where the impinging flux balances the leaving flux ($Z_{\downarrow}=Z_{\uparrow}$). Then when the shutter is closed ($t=t_2$), there is an abrupt decrease of the recorded signal to $(1-\alpha_{\theta})Z_{\downarrow}$ (where now α_{θ} is the sticking coefficient for the surface coverage θ in the steady state) and after a transitory period the signal vanishes ($t=t_3$) since the $(1-\alpha_{\theta})Z_{\downarrow}$ fraction of the reflected flux can no longer be reflected in the absence of the impinging flux Z_{\downarrow} . In such a reversible adsorption/desorption regime, the steady state is a true equilibrium state so that the shaded areas in Fig. 1(b) are proportional to the adsorbed (θ_{ad}) and desorbed (θ_{des}) quantities with furthermore, since equilibrium, $\theta_{ad}=\theta_{des}\equiv\theta$. The steady-state signal $Z_{eq}=Z_{\uparrow}=Z_{\downarrow}$ gives access to the equilibrium pressure $P_{eq}=Z_{eq}\sqrt{2\pi mkT}$. A single experiment thus gives access to the adsorption and desorption kinetics (signal evolution versus time during the transitory parts), to the surface coverage θ_{eq} (at equilibrium), and to the equilibrium pressure P_{eq} .

III. DESCRIPTION OF THE ADSORPTION AND DESORPTION MECHANISM

A. Characterization of the desorbed species: Evidence for three temperature domains

Thanks to the knowledge of the dissociation coefficient of our MS (a ratio $Z_{Sb}/Z_{Sb_2}\approx 1.5\pm 0.1$ is recorded for a pure Sb_4 flux), it is possible to identify the various desorbed or

reflected Sb_n species versus the substrate temperature. For this purpose, the surface is submitted to an impinging Sb_4 flux and the Sb_n signals are recorded by the MS in the presence of the incoming flux. In Fig. 2 we report the intensities Z_{Sb_2} and Z_{Sb} (arbitrary units) of the steady-state signal measured by the MS for Sb_2 molecules and Sb atoms. We never detect Sb_3 molecules. More precisely, we report in Figs. 2(a) and 2(b) the data obtained for two different impinging fluxes. For both fluxes, three temperature ranges are put in evidence. In the low temperature range [LT in Figs. 2(a) and 2(b)] the Sb_2 signal has a maximum constant value while the Sb signal remains minimum. In the intermediate temperature range [IT in Figs. 2(a) and 2(b)], the Sb_2 signal decreases while the Sb signal increases. Then in the high temperature range [HT in Figs. 2(a) and 2(b)] the Sb signal reaches a maximum constant value while the Sb_2 signal vanishes. These complementary results for Sb and Sb_2 species can be easily understood. Indeed, in the low temperature range, the measured ratio $Z_{Sb}/Z_{Sb_2}\approx 1.5\pm 0.1$ is characteristic of a pure Sb_4 flux (see Sec. II) that means that only Sb_4 species leave the surface. In the high temperature range, only Sb atoms are detected, so that (since there are no Sb monomers in the incident flux) only Sb monomers leave the surface. This behavior is consistent with the TDS experiments [see Fig. 1(a)]. At $T < 600$ °C there is no desorption while at $T > 600$ °C the deposited layer is desorbed.

In the following we will work in conditions of Fig. 2(b) so that $T < 600$ °C is the low temperature range and $T > 800$ °C the high temperature range. Notice that the crossing point between Sb and Sb_2 signals slightly depends upon the intensity of the impinging flux.

B. Kinetics study

The MS signals versus time have been recorded for various temperatures. We identify three temperature ranges

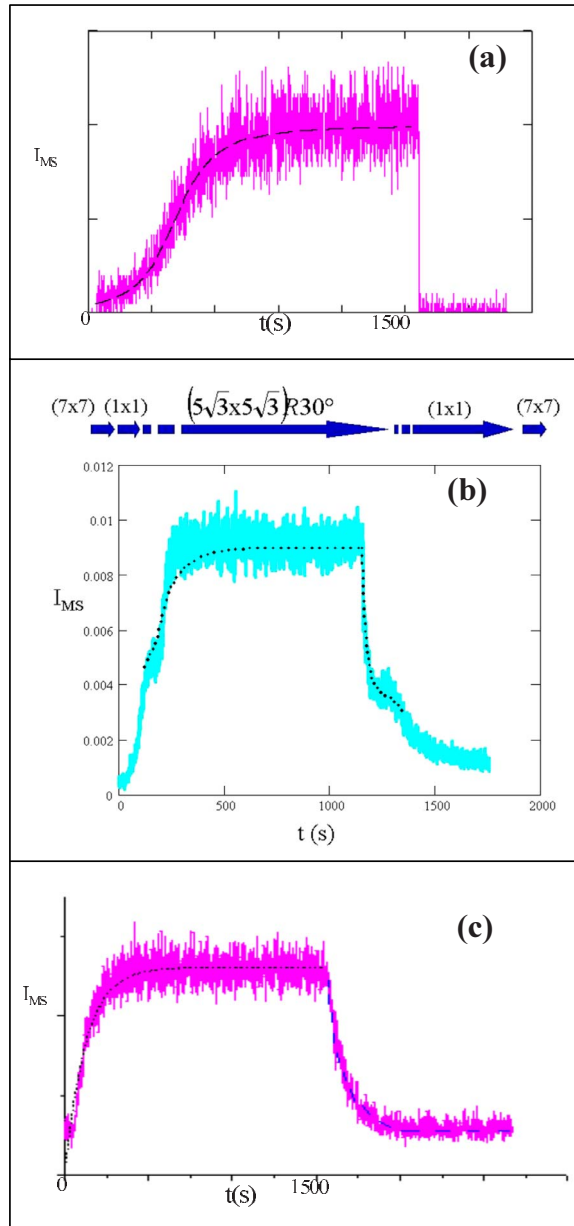


FIG. 3. (Color online) MS signal (arbitrary units) versus time recorded during the deposition at $Z_{\downarrow} = 4.8 \times 10^{11}$ at $s^{-1} cm^{-2}$: (a) $T=450$ °C, (b) 700 °C, and (c) 800 °C. The coverage in the stationary state corresponds to (a) $\theta=1$ ML, (b) $\theta=0.8$ ML, and (c) $\theta=0.5$ ML.

where kinetics curves are different. The three main behaviors are reported in Fig. 3, at low temperature [$T < 600$ °C in Fig. 3(a)], high temperature [$T > 800$ °C in Fig. 3(c)], and intermediate temperature [$600 < T < 800$ °C in Fig. 3(b)].

1. Low temperature range: Evidence for irreversible adsorption mechanism

In the low temperature range, two main characteristics have to be underlined: (i) there is a short latency period between the shutter opening and the MS species detection, and (ii) there is an abrupt decrease of the MS signal as soon

as the shutter is closed. Such behavior can be explained by considering that at low coverage (low deposit time), Sb_4 molecules are adsorbed, then dissociated into Sb monomers that cannot desorb [see again Fig. 1(a)] since $T < 600$ °C. For increasing coverage, more and more Sb_4 impinging molecules can no longer be dissociated and thus are immediately reflected by the surface. When the coverage reaches the monolayer, all the impinging Sb_4 molecules are immediately reflected by the surface so that when the flux is shut, the signal abruptly goes down to zero.

Such a mechanism implies that the sticking coefficient $\alpha(\theta)$ (defined as the ratio between the reflected Sb amount and the incident Sb amount) varies from unity to zero for increasing coverage in the submonolayer range. This mechanism can be checked by measuring the sticking coefficient versus the surface coverage for $T < 600$ °C. For this purpose we send a calibrated (by a quartz oscillator) antimony amount θ_{sent} on the Si(111) surface maintained at room temperature. Then we put the sample in front of the MS and measure the leaving flux when the so-covered surface is again exposed to an incoming flux. A sketch of $Z_{\uparrow}(t)$ curves obtained for initial coverages is given in Figs. 4(a) and 4(b). More precisely, in Fig. 4(a) the initial coverage before further exposition is roughly $\theta \approx 0.8$ ML while in Fig. 4(b) it is $\theta \approx 1$ ML. Following the procedure described in Fig. 1(b), it is thus easy to measure the sticking coefficient on such pre-covered surfaces via the abrupt increase observed at the shutter opening ($t=t_0$). It is found $\alpha(\theta=0.8) \approx 0.8$ and $\alpha(\theta=1) \approx 0.2$. In Fig. 4(c) are reported the so-measured sticking coefficients recorded for various precoverages at 450 °C. Notice that, since the sticking coefficient varies with coverage, the true adsorbed amount θ_{ad} does not coincide with the sent amount θ_{sent} . In Fig. 4(c) are reported the $\alpha(\theta_{ad})$ values obtained after numerical correction of the θ_{sent} values. As expected, the so-recorded sticking coefficient abruptly varies when approaching the monolayer. Notice that although $\alpha(\theta_{ad})$ vanishes for a monolayer, it does not completely cancel so that Sb coverage can overpass $\theta=1$ ML for giving birth to thick islands that sit on the underlying mono- or bilayer.^{13,14} Though the $\alpha(\theta_{ad})$ behavior reported in Fig. 4 has only been recorded at $T=450$ °C, it is representative of what happens for $T < 600$ °C.

The sticking coefficient behavior can be understood by revisiting the Kisliuk model¹⁹ for which the sticking coefficient reads

$$\alpha(\theta) = \frac{(1 - \theta)^n}{(1 - \theta)^n + P}, \quad (1)$$

where $P = P_b/P_a$ is an adjustable parameter describing the ratio between the desorption probability P_b of Sb_4 species and the probability P_a for a Sb_4 molecule to be chemisorbed before desorption or surface migration towards another adsorbed site. The scaling coefficient n roughly is 4 for tetramers. The continuous line in Fig. 4(c) is the fit obtained for $P = 10^{-3}$ and $n=4$.

It is then possible to use this sticking coefficient expression to simulate the kinetics behavior. For this purpose, it is

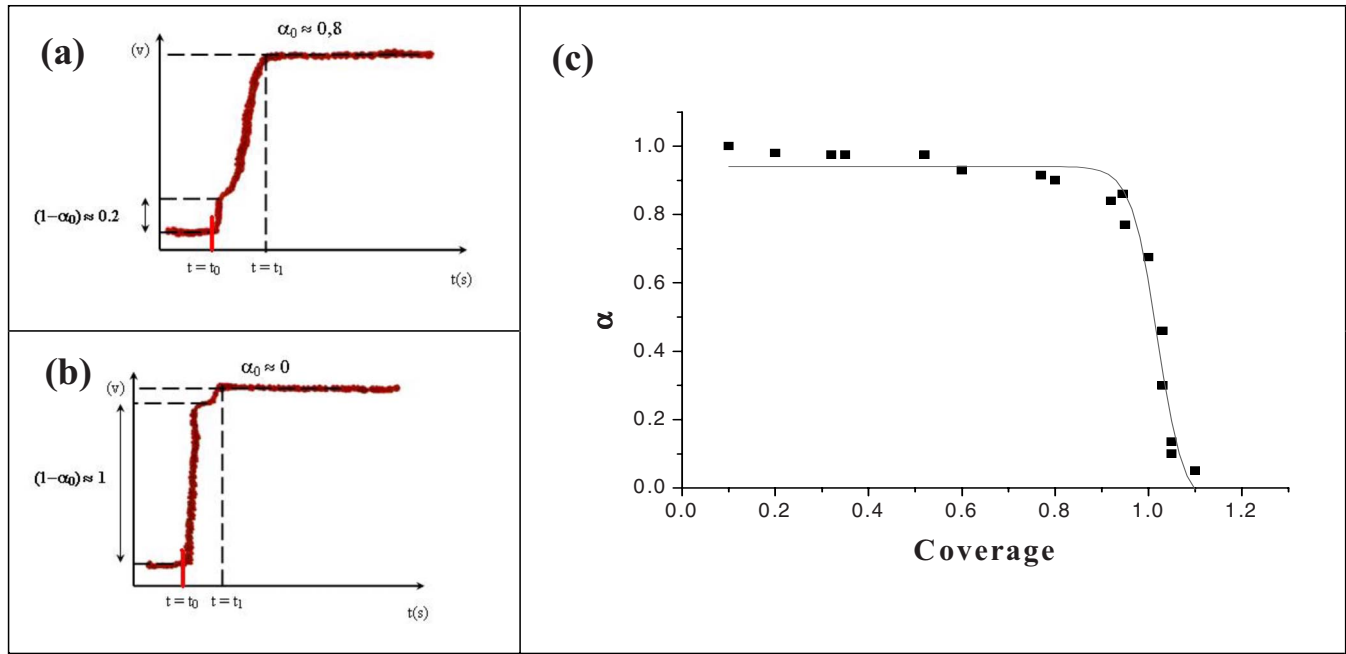


FIG. 4. (Color online) Sticking coefficient measurement: (a) MS signal recorded after predeposition of a 0.8 ML, (b) MS signal recorded after predeposition of roughly 1 ML. The abrupt signal increase $(1-\alpha_{\text{sent}})Z_{\downarrow}$ immediately gives the value of the sticking coefficient $\alpha_{\theta_{\text{sent}}}$ for the antimony amount sent on the surface. (c) Synthesis of the results showing the sticking coefficient versus coverage. The continuous line corresponds to the best-fit using Eq. (1).

enough to write the following equations giving the Sb and Sb_4 amount on the surface.

$$\begin{aligned} dn_{\text{Sb}}/dt &= 4Z_{\downarrow}\alpha(\theta), \\ dn_{\text{Sb}_4}/dt &= 0, \end{aligned} \quad (2)$$

where Z_{\downarrow} is the impinging flux (expressed in Sb_4 species) and n_{Sb} the number of adsorbed Sb atoms so that $\theta = n_{\text{Sb}}/N_S$ again is the Sb coverage expressed as a fraction of the monolayer [with N_S the number of adsorption sites on the Si(111) surface].

In this model, the signals recorded by the MS simply read (for a perfect MS in which there should be no dissociation at all) $Z_{\text{Sb}}=0$ for monomers and $Z_{\text{Sb}_4}=Z_{\downarrow}[1-\alpha(\theta)]$ for tetramers. Taking into account the dissociation phenomenon, the so-simulated results perfectly fit the experimental results [see continuous curve in Fig. 3(a)] which completely validates our kinetic model.

2. High temperature range: Evidence for reversible adsorption and desorption mechanism

At high temperature range [Fig. 3(c)] as soon as the shutter is opened, the mass spectrometer detects an increasing signal essentially corresponding to Sb species leaving the surface since $Z_{\text{Sb}_2} \approx 0$. After the steady state has been reached then the shutter closed, the Sb signal continuously vanishes. Since we only detect Sb monomers, the interpretation is quite simple: all the Sb_4 impinging tetramers are dissociated close to the surface so that the kinetics corresponds to a usual reversible adsorption/desorption mechanism. It can

thus simply be described by the following kinetic equation giving the Sb amount on the surface:

$$dn_{\text{Sb}}/dt = 4Z_{\downarrow}\alpha(\theta) - k_{\text{Sb}}n_{\text{Sb}} \quad (3)$$

where k_{Sb} is the desorption rate of Sb species which did not exist in the first equation (2) since at $T < 600$ °C there is no Sb desorption at all as shown in the TDS experiment [see again Fig. 1(a)].

The solution of Eq. (3) thus is $Z_{\text{Sb}} = \frac{4Z_{\downarrow}}{k_{\text{Sb}}}(1 - e^{-k_{\text{Sb}}t})$ for the adsorption and $Z_{\text{Sb}} = 4Z_{\downarrow}/k_{\text{Sb}}e^{-k_{\text{Sb}}t}$ for the desorption (charge and discharge of a condenser). It is thus easy to fit the experimental curves obtained at different high temperature [continuous curve in Fig. 3(c)] to obtain the unknown parameter k_{Sb} whose temperature variation gives the activation energy for desorption. We find $E=2.9$ eV in excellent agreement with other experimental results.¹²

3. Intermediate temperature range

Obviously, in the intermediate temperature range the kinetics is a mix of the two previous behaviors with partial reflection of Sb_4 species and partial desorption of Sb monomers, the ratio between both scenarios depending upon the actual temperature. Moreover, in Fig. 3(b) a stationary state also appears before and after the true equilibrium between the impinging and the leaving flux. This plateau exists as soon as $T > 600$ °C (when desorption is active) in the intermediate as well as in the high temperature range, but only for coverages greater than $\theta \approx 0.7$ ML.

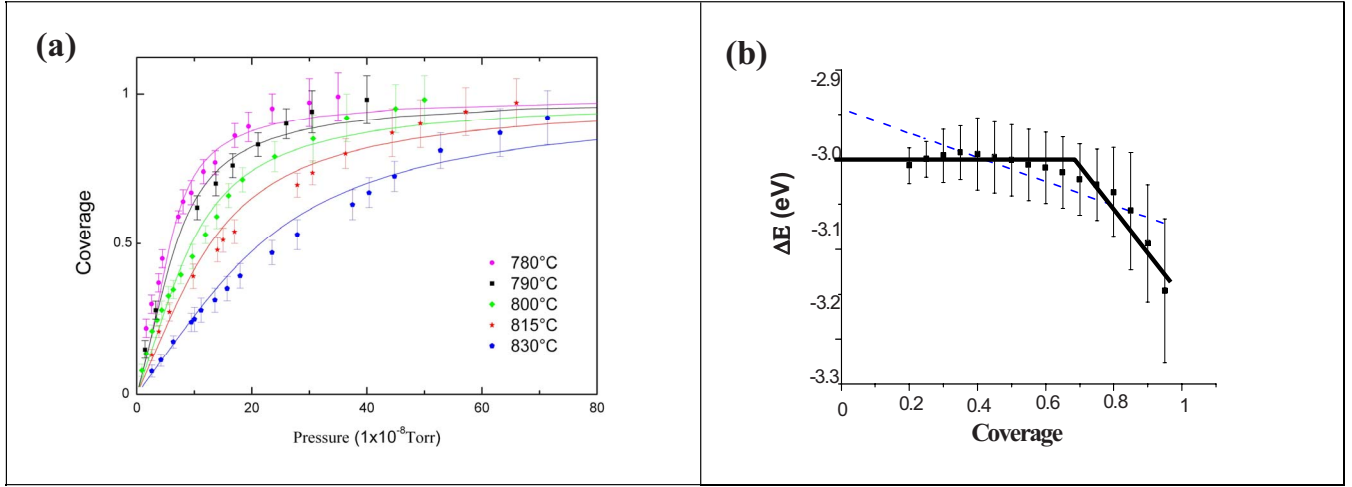


FIG. 5. (Color online) Set of experimental isotherms (a) and the deduced adsorption energy versus coverage (b). The dotted line corresponds to the mean approximation with $\Phi_{\text{SbSi}} = -2.95 \pm 0.03$ eV and $\Phi_{\text{SbSb}} = -0.02 \pm 0.006$ eV, the continuous line put in evidence the two-adsorption regimes.

4. Description of the intermediate kinetics steady state close to $\theta = 0.7$

According to their shapes, the quasistationary states that appear on the adsorption and desorption parts of kinetic curves can be interpreted as the condensation of a 2D phase on the Si surface.^{20,21} More precisely, beyond some critical density ($\theta \approx 0.7$ ML), a 2D condensation occurs. The quasistationary adsorption state thus corresponds to the condensation of a 2D phase from the 2D gas (construction of 2D islands by surface diffusion of the Sb adatom before incorporation in the island edges) whereas the quasistationary desorption state corresponds to the reverse process of dilution of the 2D dense phase (the island edges reject Sb atoms in the 2D gas phase before desorption), as described in Ref. 21. A simple kinetics model enables one to capture the essential of the physics of this 2D phase formation. For this it is enough to consider three populations: a 2D gas on the bare silicon surface (n_0 atoms), a 2D island (containing N atoms), and a 2D gas lying on the 2D island (n_1 atoms), so we can write the coupled equations

$$dn_0/dt = Z_{\downarrow}(1 - N/N_s) - k_{12}n_0\sqrt{N} + k_{21}\sqrt{N} - k_{1p}n_0,$$

$$dN/dt = k_{12}n_0\sqrt{N} - k_{21}\sqrt{N} - k_2\sqrt{N},$$

$$dn_1/dt = Z_{\downarrow}N/N_s - k_{1p}n_1,$$

where we consider a net flux from the 2D gas lying on the bare surface towards the island edges (the number of edge sites being proportional to \sqrt{N}) with the kinetic rate k_{12} and a back flux (with a kinetic rate k_{21}) from the island edge towards the 2D gas as described by Refs. 20 and 21. Furthermore, we consider that the impinging flux divides into two parts. A fraction $Z_{\downarrow}(1 - N/N_s)$ impinging on the bare silicon surface, the other $Z_{\downarrow}N/N_s$ impinging on the 2D island where N_s again is the number of surface sites on the base Si surface. The fraction of upper 2D gas lying on the 2D island desorbs with the kinetic rate k_{1p} . These coupled differential equations

can be numerically solved from a critical density of 2D gas $\theta_c = n_{0c}/N_s$. The value of θ_c is an adjustable parameter. The recorded signal thus reads $I_1 = k_{1p}n_0 + k_{1p}n_1 + k_2\sqrt{N}$. The best fit (obtained with $\theta_c = 0.5$ ML) is superimposed on Fig. 3(b).

IV. THERMODYNAMIC STUDY OF THE ADSORPTION/DESORPTION EQUILIBRIUM

We have seen in Sec. III that beyond 600 °C, reversible adsorption/desorption of Sb monomers occurs. For such a reversible adsorption/desorption regime, mass spectrometry measurements allow one to obtain, in an equilibrium situation, the adsorbed coverage ($\theta_{ad} = \theta_{des} \equiv \theta_{eq}$) and the equilibrium pressure ($P_{eq} = Z_{eq}\sqrt{2\pi mkT}$). A set of such experiments for various antimony gas pressures enables us to build an isotherm $\theta_{eq}(P_{eq})$ that we will write $\theta(P)$ for the sake of simplicity. Performing identical experiments for various surface temperatures is enough to build a set of isotherms for 750 °C < T < 850 °C (beyond the higher temperature the desorption is too quick, beneath the lower one there is a Sb₄ reflected part as shown in Fig. 4). Such an isotherms set is plotted in Fig. 5(a).

At first sight, these isotherms are sigmoid curves and thus behave as Langmuir isotherms resulting from noninteracting molecules adsorbed on definite surface sites. However, let us use the mean field expression of the isotherms obtained in a first nearest-neighbor model and known as the Bragg-Williams isotherm:

$$\theta/(1 - \theta) = KP \exp[(\Phi_{\text{SbSi}} + z\theta\Phi_{\text{SbSb}})/kT], \quad (4)$$

where K is a constant, Φ_{SbSi} is the mean vertical interaction between adsorbed Sb and Si underlying atoms, Φ_{SbSb} the lateral interaction between antimony adatoms in the surface plane, and $z\theta$ the mean number of Sb-Sb neighbors in the surface plane ($z=6$ is the coordination number in the surface plane). It is thus possible to write the isotherms (4) as $\theta/(1 - \theta) = KP \exp[\Phi_{ad}/kT]$ and thus to plot the quantity Φ_{ad}

$=kT[\ln(KP) - \ln \frac{\theta}{1-\theta}]$ as a function of the surface coverage. The result is given in Fig. 5(b). It is thus easy to see that for $\theta < 0.7$ ML there is a perfect Langmuir adsorption (with $\Phi_{ad} = \Phi_{SbSi} = -3.0$ eV and $\Phi_{SbSb} = 0$), while for $\theta > 0.7$ ML there is a Bragg-Williams adsorption since now $\Phi_{ad} = \Phi_{SbSi} + z\theta\Phi_{SbSb}$ with $\Phi_{SbSi} = -2.65$ eV and $\Phi_{SbSb} = -0.08$ eV. Thus beyond $\theta \approx 0.7$ ML there is an attractive interaction between Sb adatoms. Though the error bars are important, the transition from a regime without mean lateral interaction towards a regime with attractive interaction is meaningful, as will be proved without ambiguity in Sec. VI.

Let us recall that this peculiar behavior close to $\theta \approx 0.7$ ML could be linked to the critical coverage at which kinetics curves exhibit a 2D condensation [see again Fig. 3(b) and Sec. III B 4] and to the TDS experiments where beyond $\theta \approx 0.7$ ML the desorption peak splits in two components [see Fig. 1(a)]. For completeness, notice that in the work by Slijkerman *et al.*²² it is also reported, but for Sb/Si(001), a peculiar behavior close to $\theta \approx 0.7$ ML. In this case it seems to be associated to a blockage of the Sb_4 dissociation process.

V. CONNECTION WITH SURFACE STRUCTURES AND PARTIAL CONCLUSION

A. Phase diagram

The 2D condensation due to attractive interactions beyond $\theta \approx 0.7$ ML could be associated to peculiar surface structures so that it is natural to study those which appear for the Sb/Si(111) system. A large number of structural studies have been published in the desorption regime (a Sb monolayer has been deposited then the surface structures are followed during desorption) and many phases have been identified as $(5\sqrt{3} \times 5\sqrt{3})R30^\circ$, 2×1 , $(\sqrt{3} \times \sqrt{3})R30^\circ$, $(7\sqrt{3} \times 7\sqrt{3})R30^\circ$, diffuse 7×7 , etc...²²⁻²⁷ However, since working in equilibrium conditions, one has to only consider 2D equilibrium phases. In this context, the most important work is the one published by Andrieu²⁸ who shows that the surface phases that appear during adsorption are different from that one appearing during the desorption. His results essentially show that during adsorption a $(5\sqrt{3} \times 5\sqrt{3})R30^\circ$ 2D structure is observed for $T > 725^\circ\text{C}$ in a weak coverage domain close to $\theta \approx 0.7$ ML, whereas during desorption this phase is observed for a larger coverage domain ($0.5 \text{ ML} < \theta < 0.8 \text{ ML}$). This difference between adsorption and desorption is now well-understood since it has been recently shown that the $(5\sqrt{3} \times 5\sqrt{3})R30^\circ$ phase does not conserve its stoichiometry during desorption, where Si atoms can substitute to Sb atoms.²⁹ The equilibrium diagram (with equilibrated adsorption and desorption fluxes) could be obtained as the intersection between the two Andrieu kinetic diagrams. However, we tried here to directly build a true phase diagram (working in equilibrium conditions). For this purpose we have identified (by RHEED) the 2D surface structures that exist in equilibrium conditions (for the steady state in adsorption and desorption curves). Here, since from the adsorption/desorption experiments we know the equilibrium pressure at which appears the different 2D phase structures, we will present the main results under the form of a 1D equilibrium diagram.

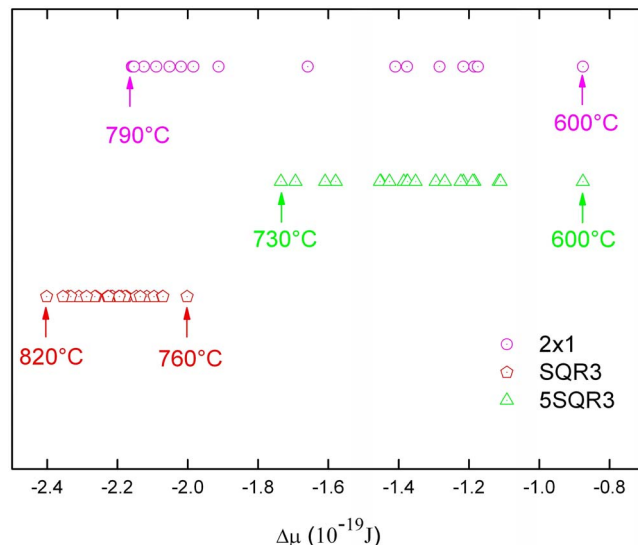


FIG. 6. (Color online) 1D phase diagrams for the three phases that exist in equilibrium conditions.

For this purpose, we calculate the thermodynamic supersaturation $\Delta\mu = kT \ln(P_{eq}/P_\infty)$ at which appears then exists a specific RHEED pattern characteristic of a peculiar reconstruction existing in equilibrium conditions. Notice that if P_{eq} is the equilibrium pressure at which exists the surface reconstruction, P_∞ is the vapor pressure of a 3D antimony crystal calculated from Ref. 30 at the working temperature. Thus $\Delta\mu$ is the antimony supersaturation with respect to a 3D infinite antimony reservoir. The results are shown in Fig. 6 for $T > 600^\circ\text{C}$ where reversible adsorption is possible.

The main results are (i) all the 2D equilibrium phases grow at undersaturation (with respect to the infinite phase) as it should be for a Frank-van der Merwe or 2D growth, (ii) at equilibrium only the $(5\sqrt{3} \times 5\sqrt{3})R30^\circ$, 2×1 , and $(\sqrt{3} \times \sqrt{3})R30^\circ$ 2D phases are observed, (iii) the $(5\sqrt{3} \times 5\sqrt{3})R30^\circ$, 2×1 phases coexist in a large domain of undersaturation in agreement with all the recent STM observations, and (iv) the $(5\sqrt{3} \times 5\sqrt{3})R30^\circ$ superstructure can only be formed in a weak undersaturation domain. STM measurements show that the 2×1 phase develops at the edge of $(5\sqrt{3} \times 5\sqrt{3})R30^\circ$ reconstructed islands.

B. Partial conclusion

The previous results enable us to perfectly describe the adsorption mechanisms in irreversible ($T < 600^\circ\text{C}$) as well as in reversible ($T > 600^\circ\text{C}$) conditions. These mechanisms result from a subtle temperature dependent competition between sticking, adsorption, and dissociation of Sb_4 molecules on one hand and Sb_4 reflected flux or Sb desorbed flux on the other hand. Moreover, a peculiar behavior appears close to a critical coverage $\theta \approx 0.7$ ML. Beneath this coverage the adsorption takes place as a Langmuir adsorption (the Sb species adsorbed on the surface do not interact and thus ignore each other), while close to this critical coverage the nature of the Sb-Sb abruptly change towards attractive interactions which leads to a 2D condensation that can clearly be seen on

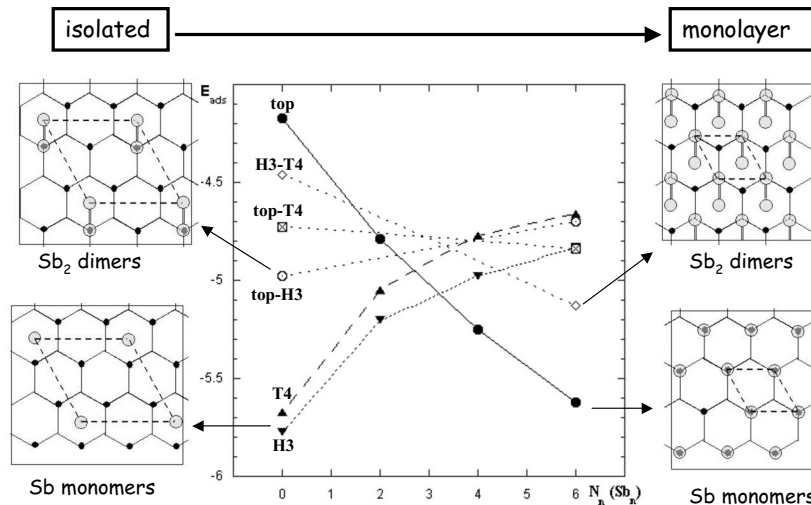


FIG. 7. Variation of the adsorption energy (E_{ads} in eV/at) for Sb and Sb_2 adsorbed species as a function of the number of Sb/ Sb_2 first neighbors $N_n(Sb_n)$. For the monomers, the Sb adatom is located on *top* (full line with dots, ●), T4 (dashed line with up triangles, ▲), and H3 (dotted line with down triangles, ▼) positions. For the dimers (small dashed lines), the Sb atoms occupy, respectively, *top*-H3 (○), *top*-T4 (◻), or H3-T4 (◇) positions. The most stable superstructures for monomers and dimers in the two limit cases (isolated, monolayer) are schematized in the insets (gray large dots: Sb adatoms, small black dots: Si surface atoms, and line intersections: Si first underlayer atoms). (For the inset: ○: Si atoms, ●: Sb atoms). Notice that in our *ab initio* calculations for dimers, $N_n(Sb_2)=0$ corresponds to $\theta=0.5$ ML and $N_n(Sb_2)=6$ corresponds to $\theta=2$ ML.

the adsorption and desorption kinetics but is partially hidden in the adsorption/desorption isotherms where no corresponding step has been evidenced. Moreover, close to this critical coverage a specific $(5\sqrt{3} \times 5\sqrt{3})R30^\circ$ 2D surface structure also appears, as well as splitting of the TDS peak.

Beyond the experimental questions, essentially due to the error bars and some experimental details described in Ref. 31, the main question is the origin of the change of the nature of the Sb-Sb interaction (from zero interaction to attraction) close to $\theta \approx 0.7$ ML. A complete understanding of this phenomenon needs an atomistic modelization of the adsorption/desorption phenomena, and thus a realist atomic potential that enables us to describe the Sb-Sb and the Sb-Si interactions. We have thus performed an *ab initio* study of the Sb/Si(111) adsorption. Nevertheless we will simplify the problem by ignoring the real surface superstructures for two main reasons: (i) from a general viewpoint the energy difference between surface structures is weak so that we believed that the driving force for changing the nature of the interaction has a more “robust” origin, and (ii) the $(5\sqrt{3} \times 5\sqrt{3})R30^\circ$ phase that appears close to the transition is in fact a “soft” phase which may admit important stoichiometry modifications without any structural change.²⁹ A second simplification will be to ignore the temperature effect and thus to work only at zero K. Such a simplified *ab initio* simulation of the Sb/Si(111) system is the goal of the next section.

VI. AB INITIO STUDY OF Sb/Si(111) ADSORPTION

As summarized at the end of the previous section, the experimental results collected on the Sb/Si(111) interface have raised many questions, particularly about the influence of Sb coverage on:

(1) The nature of Sb adsorption at the surface: molecular or dissociative adsorption?

(2) The nature of adsorbed Sb particle interactions: attractive or repulsive?

(3) The organization of the various Sb superstructures identified by RHEED-STM?

To answer these questions, we have performed *ab initio* calculations of the energy of the Sb/Si(111) system for adsorption of Sb_n species (here $n=1$ for monomers and $n=2$ for dimers) in the two limit cases of isolated Sb_n species and completion of a Sb_n monolayer. Let us explain that our aim here is not to describe the kinetics of the adsorption (which among others would require one to include Sb_4 molecules) but to characterize the thermodynamic equilibrium state, which has been experimentally shown to involve only Sb and Sb_2 species.

The calculations have been performed using the WIEN97 full-potential linearized augmented wave planes (FP-LAPW) package in the local density approximation (LDA) for the exchange potential. The Sb/Si(111) system has been simulated by a periodic slab of Si layers, with Sb atoms on each side, separated by vacuum layers in order to avoid interactions between the covered layers. The Si surface is a perfect (111) surface with three main adsorption sites: the *top* site and two ternary sites occupying respectively, fcc (hollow site H3) and hcp (ternary site T4) positions (see insets of Figs. 7 and 8). The unit cell used for describing intermediate coverages between isolated Sb_n entities and full Sb_n monolayers is the 2×2 unit cell described in Fig. 7. In view of the size of this unit cell it has been necessary to reduce the thickness of the slab to get reasonable computational time. We have checked that three Si bilayers separated by six vacuum layers was enough to recover the same energy in the midlayer of the slab for all the adsorption configurations under study.³¹ In what concerns the computational parameters it was essential to properly determine both the cutoff of the plane waves (k_{max}), which controls the size of the plane-wave basis, and

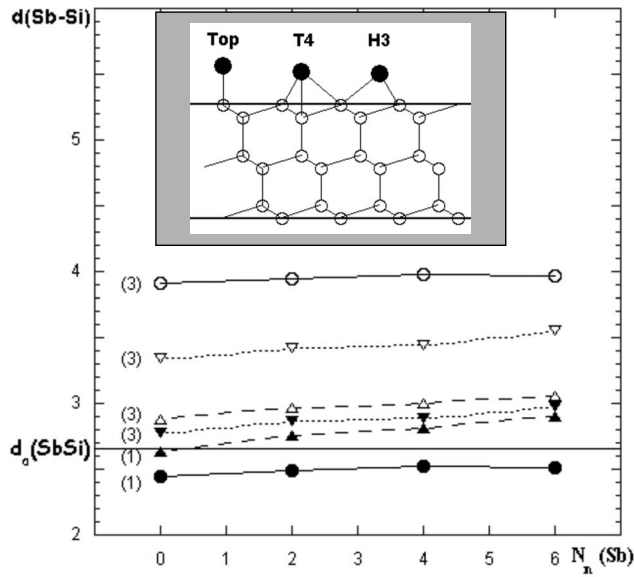


FIG. 8. Variation of the Sb-Si distance [$d(\text{Sb-Si})$ in Å] for Sb adsorption as a function of the number of Sb first neighbors $N_n(\text{Sb})$, depending on that the adatom occupies the *top* (full line with dots ●,○), T4 (dashed line with up triangles ▲,△), or H3 (dotted line with down triangles ▼,▽) positions. For the sake of comparison the Sb-Si average bulk interatomic distance $d_a(\text{SbSi})$ is also recalled. The different coordination numbers are given in parenthesis. In the inset the three adsorption sites are schematized.

N_k the number of k points used for the integration in the Brillouin zone. The parameter k_{max} has to be sufficiently large to ensure convergence but not too much in order to be not too time consuming. The same problem arises for N_k which has also to be sufficiently large to account properly for the evolution of the local density of states but still not too much. Thus varying N_k between 10 and 1000 and the adimensional parameter $R_{mt}k_{\text{max}}$ (where R_{mt} is the muffin-tin radius) between 6 and 9, we have checked that $N_k=100$ and $R_{mt}k_{\text{max}}=7$ are sufficient to reach convergence of the total energy in the Brillouin zone.³¹ In practice, the criterion used to compare the respective stabilities of the various entities present at the surface (Sb monomers adsorbed on one of the three adsorption sites: top, T4, and H3 sites or Sb_2 dimers adsorbed in mixed situations, the two Sb adatoms occupying different adsorption sites: top-H3, top-T4, H3-T4) for a given coverage (here isolated or monolayer) is to minimize the adsorption energy per Sb atom defined as

$$E_{\text{ads}} = \frac{E_{\text{tot}}(\text{Sb/Si}) - E_{\text{tot}}[\text{Si}(111)]}{N_{\text{Sb}}} - E_{\text{isol}}(\text{Sb}), \quad (5)$$

where $E_{\text{tot}}(\text{Sb/Si})$ and $E_{\text{tot}}[\text{Si}(111)]$ are the total energies of the Si(111) slabs, respectively, covered or uncovered by Sb atoms and $E_{\text{isol}}(\text{Sb})$ the energy of the isolated Sb atoms calculated as the asymptotic value of the bulk energy when the interatomic distances are sufficiently expanded. Notice that within this definition, the initial state is the same for both monomers and dimers, namely a gas of isolated Sb atoms. Indeed this is the only way to properly determine the respective stabilities of adsorbed Sb and Sb_2 from the direct comparison of their adsorption energies (per atom). Let us underline that our problem being essentially two-dimensional, here we will only relax the vertical distances Sb-Si. This means that the Si substrate is frozen during all the procedures. Then, for the Sb_2 dimers, the adsorption energies have been calculated by a n-step process in which the Sb-Si distance of both Sb adatoms have been alternatively relaxed until an energy minimum has been reached. We have checked in a few cases that allowing slight horizontal displacements with respect to the three ideal positions do not change quantitatively the main results.

The adsorption energies for Sb_n monomers and dimers either isolated [no Sb_n neighbors: $N_n(\text{Sb}_n)=0$] or organized in a (1×1) condensed phase [six Sb_n neighbors occupying the same adsorption lattice $N_n(\text{Sb}_n)=6$] are synthesized in Fig. 7 and Table I. Note that these two limit cases have already been reported elsewhere for Sb monomers,¹⁴ but that they have been completed here by calculations for intermediate coverages corresponding to $N_n(\text{Sb}_n)=2, 4$, and by those for dimers. This figure deserves many comments. The first one concerns the respective stabilities of Sb monomers and dimers. One can see that, whatever the coverage [at least below completion of Sb monolayer, $\theta=1$ ML which corresponds to $N_n(\text{Sb})=6$], the adsorption is dissociative since the minimum value for monomers is, in all cases, below that for dimers. However, thanks to the fact that the Si(111) surface is not a close-packed plane, the Sb coverage can now vary from $\theta=0$ to 2 ML. Then, for $\theta > 1$ ML, this figure shows that additional Sb adatoms are incorporated in first neighbor positions of the Sb atoms already present at the surface, leading to organized Sb_2 structures. A more compact ad-layer ($\theta=2$ ML) is thus reached for a mixed situation in which only H3 and T4 sites are occupied.

TABLE I. Adsorption energies (in eV/atom) for the three possible positions of Sb monomers and Sb_2 dimers in both limits: isolated entities or full monolayer.

	Monomers			Dimers		
	Top	T4	H3	Top-T4	Top-H3	T4-H3
$N_n(\text{Sb}_n)=0$ Isolated n-mers	-4.17	-5.67	-5.77	-4.73	-4.98	-4.46
$N_n(\text{Sb}_n)=6$ Full n-mers monolayer	-5.62	-4.56	-4.83	-4.84	-4.70	-5.13

The second comment concerns the coverage dependence of the adsorption energy for each species first, and then from one to the other species. Let us first describe the case of Sb monomers (which corresponds to the most stable situation for $\theta < 1$ ML). In that case, one observes a spectacular reversal of the adsorption site from ternary towards *on top* site as a function of increasing coverage, the transition occurring around $\theta \approx 0.7$ ML [$N_n(\text{Sb}_2) \sim 3$]. The difference between the H3 and T4 site is very weak so that it could be inverted by simple entropic considerations at nonzero temperature. The existence of such a transition is closely linked to the different nature of Sb interactions depending on that they are observed on ternary or on top sites. Indeed, these interactions are found repulsive (positive slope) in the former case whereas they are found attractive (negative slope) in the latter case. Then, beyond $\theta = 1$ ML, dimers begin to be stabilized on the surface. There again, the nature of the interaction between Sb_2 dimers strongly depends on their location: repulsive for top-H3 dimers, vanishing for top-T4 ones, and finally attractive for H3-T4 ones. Note that the situation is somewhat reversed with respect to the case of monomers since now, dimer interactions are repulsive for those involving one *on top* position whereas they are attractive for those adsorbed on ternary positions only. This behavior obviously leads to a site reversal from mixed (top-ternary) sites at low dimer coverage to pure ternary ones for a higher one, the transition taking place at about $\theta = 1.3$ ML [corresponding to $N_n(\text{Sb}_2) \sim 3$]. The global scenario of adsorption as a function of coverage suggests that two phase transitions can be expected for this system. These results enable us to describe the adlayer structure versus coverage. For weak coverages, the adsorption is dissociative and Sb monomers repel one another in ternary sites. A structural transition towards *on top* sites on which monomers now attract one another occurs at $\theta \sim 0.7$ ML. This transition explains the two regimes derived from the measured isotherms, as well as the formation of condensed phase beyond the transition coverage. Then for high enough supersaturations, it is possible to overpass $\theta = 1$ ML to form dimers. After a short range in which dimers partially located on top sites repel one the other, a second transition occurs around $\theta = 1.3$ ML towards condensed phases of dimers occupying both H3 and T4 sites.

Let us add that, despite the natural tendency towards phase separation of the bulk SbSi alloys, we have also checked the possible Sb incorporation (by substitution) in the first Si layer. For this purpose we have calculated the substitution energy as the difference between the energy of the system in which N_{Sb} silicon atoms have been replaced by Sb atoms and the initial system constituted by the Si(111) layer and Sb species only in the vapor. The Si atoms, after substitution, have been considered to incorporate kink position and thus have the same energy as that in the bulk. We have found that incorporation energies have the same order of magnitude as the adsorption energies, so that a possible competition between adsorption and incorporation is possible. However, because the reference energies are not the same for adsorption and substitution, they cannot be directly compared. Moreover, the incorporation energies decrease with coverage (the result is not shown here but can be found in Ref. 31). It means if incorporation occurs, it takes place without any

change in the nature of the Sb-Sb interactions. However notice that, within error bars, experiments show that there is, at equilibrium $\theta_{ad} \approx \theta_{des} \equiv \theta$, so that, in practice, incorporation seems to play only a second role.

Coming back to adsorption, it is obvious that all these situations lead to geometrically different situations. Let us now consider the variation of the vertical Sb-Si distance versus coverage, first for monomers (Fig. 8), then for dimers (Fig. 9). In the latter case, the Sb-Sb length of the molecule is also reported in Fig. 9. All these distances are the ones calculated for the minimal adsorption energies. Let us first comment on the evolution for Sb monomers. It is easy to see in Fig. 8 that the equilibrium distance changes with the nature of the adsorption site, that in all the cases the vertical distance increases with coverage, and that the smallest Sb-Si distance is the apical one whatever its stability with respect to the ternary situation. All these features can be easily understood. The Sb-Si distance globally increases with coverage because of the weakening of the vertical bonding due to the increase of the number of lateral bondings (the electrons being shared among more neighbors). Considering the number of Sb neighbors for various coverages in each adsorption lattice, it is also easy to understand that the driving force for the selection of the adsorption site in fact is the maximization of the number of Sb neighbors. More precisely, the Sb atom which prefers to be surrounded by six nearest neighbors (in fact three shorter and three larger distances) in Sb bulk crystal tries to minimize its number of Si neighbors when already surrounded by six Sb atoms ($\theta = 1$ ML, on top position) and on the contrary to maximize it when isolated (weak θ values in the ternary position). All along the adsorption from the isolated Sb towards the Sb monolayer, the equilibrium distance remains close to the average distance between Sb and Si bulk.

The situation is a little bit more complex in what concerns the geometrical structure adopted by Sb_2 dimers. Figure 9 illustrates how the length [$d(\text{Sb-Sb})$] of the dimer and its distances to its first Si neighbors [$d(\text{Sb-Si})$] evolve with both its adsorption sites [top-H3 (a), top-T4 (b), and H3-T4 (c)] and coverage (from isolated dimers to full monolayer). More precisely, the completion $\theta = 2$ ML is reached when the most stable dimer (H3-T4, see Fig. 7) recovers a distance close to the equilibrium Sb-Sb distance in Sb bulk (note that it is also the case for the top-T4 dimer). Moreover, following the variation of the Sb-Si distances from the isolated dimer to the full monolayer for the two corresponding stable modes [see shaded areas in Figs. 9(a) and 9(c)] brings information on the mechanism by which the site transition occurs from top-H3 for low coverages ($1 \text{ ML} < \theta < 1.3 \text{ ML}$) toward H3-T4 at completion ($\theta = 2$ ML). This is more clearly illustrated in the top part of Fig. 9, in which one can see that when the coverage increases the Sb_2 molecule stands up, keeping one atom located in a quasiunchanged hollow (H3) position, while the other changes from a top toward a more higher T4 position. In other words, the second Sb monolayer starts to grow at $\theta = 1.3$ ML to achieve a perfect bilayer at $\theta = 2$ ML. As already noticed, the interatomic Sb-Sb distance in the final quasivertical Sb_2 molecule is equal to that in Sb bulk. In fact, at $\theta = 2$ ML, the Sb_2 molecule can be considered as sitting quasiperpendicularly to the surface in the hol-

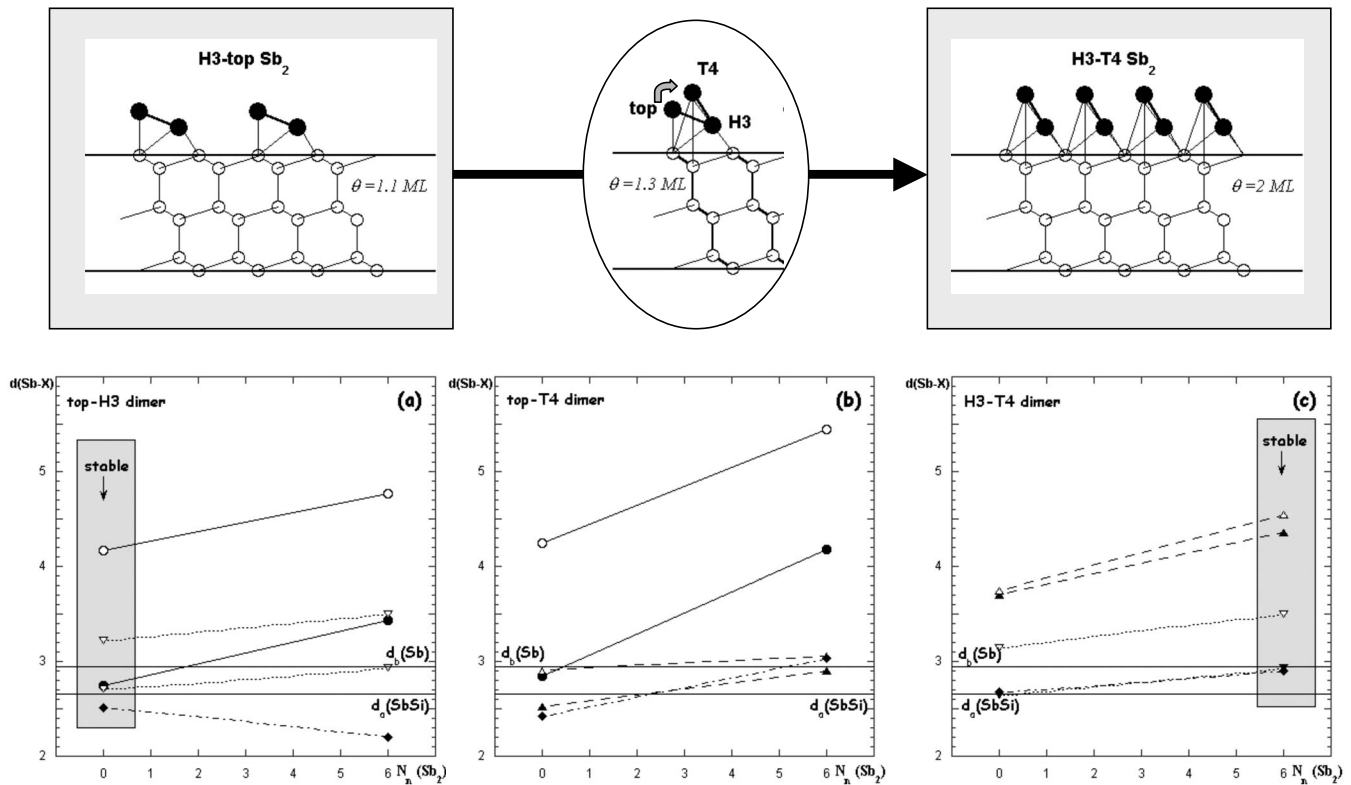


FIG. 9. Variation of the Sb-X ($X=\text{Si,Sb}$) distance [$d(\text{Sb-X})$ in Å] for Sb_2 dimer adsorption as a function of the number of Sb_2 first neighbors $N_n(\text{Sb}_2)$, depending on that the dimer occupies *top*-H3 (a), *top*-T4 (b), or H3-T4 (c) positions. The full line with dots (\bullet, \circ) refers to the Sb-Si neighbor distance for Sb in the *top* position, the dashed line with up triangles ($\blacktriangle, \triangle$) for Sb in the T4 position, and the dotted line with down triangles ($\blacktriangledown, \triangledown$) for Sb in the H3 position. Finally the dashed-dotted line with diamonds (\blacklozenge) corresponds to the Sb_2 length. For the sake of comparison the Sb bulk interatomic distance $d_b(\text{Sb})$ and the average between bulk Si at Sb distances $d_a(\text{SbSi})$ are also recalled. The gray shaded areas indicate the most stable positions, which are illustrated above (\circ : Si atoms, \bullet : Sb atoms). The transition mechanism from the horizontal to vertical position is schematized in the inset. Let us recall that for dimers, $N_n(\text{Sb}_2)=0$ corresponds to $\theta=0.5 \text{ ML}$ and $N_n(\text{Sb}_2)=6$ corresponds to $\theta=2 \text{ ML}$.

low site, as in the case of adsorption at steps,^{13,14} which could indicate a more complex situation in the latter situation than previously thought.

From the point of view of the electronic structures, one also observes drastic changes, which are at the origin of the structural transitions described above. In particular, a look at the local densities of states^{13,31} shows that the stability of the on-top site for the monomer at completion originates from the disappearance of the surface state which appears in the bulk gap for a clean Si(111) surface on this site whereas it persists for complete adsorption in ternary sites. This passivation thus enhances the stability of on-top sites. Adsorption on ternary sites (not shown) does not lead to the disappearance of the surface states. Our calculations also allow us to calculate the charge transfer. For this purpose, thanks to the “muffin-tin” geometry we use for our LAPW calculations, we can calculate the number of electrons at the Fermi level inside the atomic spheres and in the interstitial zone for Si and for Sb in the various considered configurations. In all cases, we find an electron transfer from Si towards Sb atoms, larger for on-top positions ($\Delta n \sim 0.6$) than ternary ones ($\Delta n \sim 0.4$), which could allow one to discriminate between these sites in core level photoemission experiments.

VII. CONCLUSION

The adsorption mechanisms result from a subtle temperature dependent competition between sticking, adsorption, and dissociation of Sb_4 molecules from one hand and Sb_4 reflected flux or Sb desorbed flux on the other hand. The leading term strongly depends upon the temperature range. At high enough temperature, there is some critical coverage $\theta \approx 0.7$ beyond which the nature of the Sb-Sb interaction abruptly changes and thus leads to a 2D condensation characterized by a specific kinetics signature but hidden in the adsorption/desorption isotherms. The *ab initio* study of the Sb/Si(111) adsorption provides us with a deep understanding of the underlying mechanisms. The nature of the adsorption site changes versus coverage from ternary towards the on-top position and the character of the Sb-Sb effective interactions changes from repulsive towards attractive. Moreover, it allows us to make some predictions. In particular it is possible to overpass $\theta=1 \text{ ML}$ by the formation of dimers, first partially located on top sites, up to a second phase transition around $\theta=1.3 \text{ ML}$ in which dimers leave the on top sites and stand up for building the second Sb layer.

Beyond these specific results, which illustrate the richness of this system and allow us to have a good understanding of

the adsorption and desorption mechanisms, we would like to point out some discrepancies and/or perspectives.

(1) Though experimental and theoretical results perfectly agree, some weak discrepancies between experiments and theoretical calculations still exist. This essentially concerns the fact that if experiments evidence a transition at $\theta \approx 0.7$ from zero Sb-Sb in-plane interaction towards attractive interaction, it is not exactly the case in calculations which predict a transition (also at $\theta \approx 0.7$), but from repulsive to attractive. We believe that this discrepancy originates from the fact that the transition in fact is quite continuous so that on the surface for $\theta < 0.7$ domains coexist with adsorption on ternary sites and adsorption on top sites. The mean interactions thus remain more or less zero from an experimental point of view. Such a scenario implies that from a statistical viewpoint, the local fluctuations of coverage can lead to a local dense island (with on-top adsorption) coexisting with a 2D diluted phase (ternary sites). Such a scenario can only be checked by Monte Carlo simulations in the grand canonical ensemble. It will be our future task. The Monte Carlo simulations will also give new information concerning the second phase transition expected for $\theta > 1.3$ ML. This second transition could also be experimentally studied by using higher antimony pressure and thus higher supersaturation.

(2) From the viewpoint of the applications, the set of isotherms enable us to obtain the surface energy variation $\Delta\gamma$ as a function of the antimony coverage θ . More precisely, a simple integration of the isotherms gives, by using the Gibbs isotherms formulation, $\Delta\gamma(\theta)$ given in Fig. 10. The pure surfactant effect of antimony onto Si growth is thus quantified. Obviously, as theoretically shown from a general viewpoint in Ref. 32 and experimentally observed for Sb/Si(111) in Refs. 33 and 34, the surface stress variation with the antimony coverage may also contribute to the surfactant effect.

(3) From a fundamental viewpoint it is believed that the situation in which the nature of the adsorbate-adsorbate in-

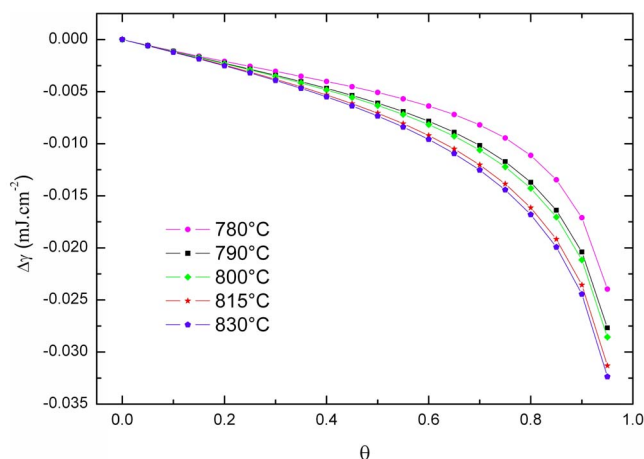


FIG. 10. (Color online) Variation of the surface energy density of the Si(111) surface as a function of the antimony coverage obtained by integration of the isotherms.

plane interactions strongly changes with coverage should be a more general behavior. It could be observed for all the systems where the adsorbed species do not present a close-packed bulk structure, so that the tendency of the systems to maximize or not their bonds with the substrate evolves with coverage. More generally, such a behavior could be the rule more than the exception each time that chemical (adsorption, segregation) and structural (reconstructions, adsorption lattice) segregations interplay, as recently shown, for instance, in the Ag/Cu system.³⁵

ACKNOWLEDGMENTS

We are strongly indebted to B. Legrand, A. Saúl, and A. Ranguis for their invaluable help. F. Leroy is also acknowledged for critical reading.

*Present address: Institut Charles Gerhardt, UMR 5253-CNRS-Ecole de chimie de Montpellier, 34295 Montpellier, France.

¹V. König, E. Kasper, and H. Herzog, *J. Cryst. Growth* **52**, 151 (1981).

²B. Voigtlander, A. Zinner, T. Weber, and H. P. Bonzel, *Phys. Rev. B* **51**, 7583 (1995).

³S. Barnett, H. Winters, and J. Greene, *Surf. Sci.* **165**, 303 (1986).

⁴M. Richter, J. C. Woicik, J. Nogami, P. Pianetta, K. E. Miyano, A. A. Baski, T. Kendelewicz, C. E. Bouldin, W. E. Spicer, C. F. Quate, and I. Lindau, *Phys. Rev. Lett.* **65**, 3417 (1990).

⁵J. Nogami, A. Baski, and C. Quate, *Appl. Phys. Lett.* **58**, 475 (1991).

⁶R. A. Metzger and F. G. Allen, *Surf. Sci.* **137**, 397 (1984).

⁷S. Andrieu and F. Arnaud d'Avitaya, *Surf. Sci.* **219**, 277 (1989).

⁸V. K. Paliwal, A. G. Vedeshwar, and S. M. Shivaprasad, *Phys. Rev. B* **66**, 245404 (2002).

⁹H. B. Elswijk, D. Dijkamp, and E. J. V. Loenon, *Phys. Rev. B* **44**, 3802 (1991).

¹⁰R. G. Ryland, S. Hasegawa, and E. D. Williams, *Surf. Sci.* **345**,

22 (1996).

¹¹Y. Kusumi, K. Fujita, and M. Ichikawa, *Surf. Sci.* **372**, 28 (1997).

¹²S. Shivaprasad, V. Paliwal, and A. Chaudhuri, *Appl. Surf. Sci.* **237**, 93 (2004).

¹³M. Ladevèze, G. Tréglia, P. Müller, and F. A. D'Avitaya, *Surf. Sci.* **395**, 317 (1998).

¹⁴P. Müller, A. Ranguis, M. Ladevèze, F. Arnaud d'Avitaya, and G. Tréglia, *Surf. Sci.* **417**, 107 (1998).

¹⁵L. Lapena, P. Müller, G. Quentel, H. Guesmi, and G. Tréglia, *Appl. Surf. Sci.* **212-213**, 715 (2003).

¹⁶H. Guesmi, L. Lapena, A. Ranguis, P. Müller, and G. Tréglia, *Phys. Rev. Lett.* **94**, 076101 (2005).

¹⁷H. Guesmi, L. Lapena, P. Müller, and G. Tréglia, (unpublished).

¹⁸P. Müller, R. Kern, A. Ranguis, and G. Zerwetz, *Europhys. Lett.* **26**, 461 (1994).

¹⁹J. Kisliuk, *J. Phys. Chem. Solids* **3**, 95 (1957).

²⁰R. Kern and G. Lelay, *J. Phys. (Paris), Colloq.* **38**, 155 (1977).

²¹R. Kern, J. Métois, and G. Lelay, in *Current Topic in Material Science Vol. 3*, edited by E. Kaldis (North-Holland, Amsterdam,

- 1979), pp. 131–419.
- ²²W. Slijkerman, P. Zagwijn, J. van der Veen, D. Gravesteijn, and G. van de Walle, *Surf. Sci.* **262**, 25 (1992).
- ²³M. Tabe and K. Kajiyama, *Jpn. J. Appl. Phys., Part 1* **22**, 423 (1983).
- ²⁴C. Y. Park, T. Abukawa, T. Kinoshita, Y. Enta, and S. Kono, *Jpn. J. Appl. Phys., Part 1* **27**, 147 (1988).
- ²⁵H. B. Elswijk, D. Dijkkamp, and E. J. van Loenen, *Phys. Rev. B* **44**, 3802 (1991).
- ²⁶R. G. Ryland, S. Hasegawa, and E. D. Williams, *Surf. Sci.* **345**, 22 (1996).
- ²⁷Y. Kusumi, K. Fujita, and M. Ichikawa, *Surf. Sci.* **372**, 28 (1997).
- ²⁸S. Andrieu, *J. Appl. Phys.* **69**, 1366 (1991).
- ²⁹A. Saranin, A. V. Zotov, V. G. Lifshits, O. Kubo, T. Harada, M. Katayama, and K. Oura, *Surf. Sci.* **447**, 15 (2000).
- ³⁰R. Honig, *RCA Rev.* **3**, 567 (1962).
- ³¹H. Guesmi, Ph.D. thesis, University Paul Cezanne Aix Marseille III, 11 Juillet 2005, <http://www.crmcn.univ-mrs.fr/gModel/index.php?id=fr&pg=Thesis>
- ³²P. Müller and R. Kern, *Appl. Surf. Sci.* **102**, 6 (1996).
- ³³P. Zahl, P. Kury, and M. Horn von Hoegen, *Appl. Phys. A: Mater. Sci. Process.* **69**, 481 (1999).
- ³⁴P. Kury, P. Zahl, and M. Horn von Hoegen, *Anal. Bioanal. Chem.* **379**, 582 (2004).
- ³⁵I. Braems, F. Berthier, J. Creuze, R. Tétot, and B. Legrand, *Phys. Rev. B* **74**, 113406 (2006).